ACS APPLIED MATERIALS & INTERFACES

Research Article

www.acsami.org

Co-Doped Branched ZnO Nanowires for Ultraselective and Sensitive Detection of Xylene

Hyung-Sik Woo,[†] Chang-Hoon Kwak,[†] Jae-Ho Chung,[‡] and Jong-Heun Lee*,[†]

[†]Department of Materials Science and Engineering, Korea University, Seoul, 136-713, Republic of Korea

[‡]Department of Physics, Korea University, Seoul, 136-713, Republic of Korea

Supporting Information

ABSTRACT: Co-doped branched ZnO nanowires were prepared by multistep vapor-phase reactions for the ultraselective and sensitive detection of *p*-xylene. Highly crystalline ZnO NWs were transformed into CoO NWs by thermal evaporation of $CoCl_2$ powder at 700 °C. The Co-doped ZnO branches were grown subsequently by thermal evaporation of Zn metal powder at 500 °C using CoO NWs as catalyst. The response (resistance ratio) of the Co-doped branched ZnO NW network sensor to 5 ppm *p*-xylene at 400 °C was 19.55, which was significantly higher than those to 5 ppm toluene, C_2H_5OH, and other interference gases. The sensitive and selective detection of *p*-xylene, particularly distinguishing among benzene, toluene, and xylene with lower cross-responses to C_2H_5OH, can be attributed to the tuned catalytic activity of Co components, which induces preferential dissociation of *p*-xylene into more active species, as well as the increase of chemiresistive variation due to the abundant formation of Schottky barriers between the branches.

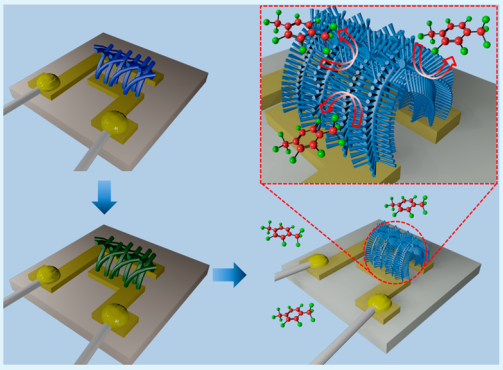

KEYWORDS: *gas sensor, Co-doping, ZnO nanowires, selectivity, xylene*

1. INTRODUCTION

Volatile organic compounds (VOCs), such as benzene, xylene, toluene, HCHO, and C_2H_5OH, are representative harmful indoor pollutants and are strictly regulated by law in many countries. They usually have a long-term effect on human health, because they exist in low concentrations and the symptoms tend to develop gradually. For this reason, it is an important issue to detect low concentrations of indoor VOCs. The simple and cost-effective detection of indoor pollutants by either hand-held and/or miniaturized monitoring devices is essential for universal usage. Although analytical methods such as gas chromatography−mass spectroscopy[1] and fluorescence spectroscopy[2] can facilitate precise detection and measurement of VOCs, they usually require expensive equipment and prolonged sample preparation time. If the selective and sensitive detection of VOCs is possible using metal oxide semiconductors, it will be advantageous for the mass fabrication of miniaturized, low-cost, and rapid-responding gas sensors. Among the various VOCs, aromatic hydrocarbons, such as benzene, toluene, and xylene (BTX), are usually difficult to detect by means of oxide semiconductor gas sensors due to their relatively low reactivity. In addition, the selective detection of a single gas among BTX is a much more challenging and important task because of their similar chemical properties, but different effects on human health. Accordingly, the precise distinction between BTX is essential in order to find a proper countermeasure for a specific pollutant.

ZnO is a typical n-type semiconductor with a band gap of 3.37 eV and has been widely investigated in the fields of electronics, optics, photonics, and gas sensors. ZnO is also known to be a versatile nanomaterial with various growth morphologies and growth surfaces, such as nanowires, nanorods, nanobelts, nanocombs, nanorings, nanocages, and nanosprings. Although ZnO gas sensors are relatively common in the literature, the high response to reactive C_2H_5OH gas has limited their use for the selective detection of aromatic hydrocarbons.[3,4] Therefore, the doping or surface modification of ZnO using catalytic materials can be considered as an effective approach to achieve sensitive and selective detection of VOCs, particularly important in the case of BTX gases.

n-Type metal oxide semiconductors, such as SnO_2, ZnO, In_2O_3, and Fe_2O_3, have been widely studied for the application of semiconductor gas sensors because of their higher gas response compared to p-type metal oxides.[5] However, p-type metal oxide semiconductors have been receiving much attention for their unique catalytic properties and higher oxygen adsorption due to their multivalence properties, which make them good candidate materials for the selective detection of large molecule VOCs. In particular, among various p-type metal oxides, Co_3O_4 is known to be an excellent catalyst for the oxidation of xylene in the liquid and vapor states.[6−9]

Received: September 29, 2014
Accepted: November 24, 2014
Published: November 24, 2014

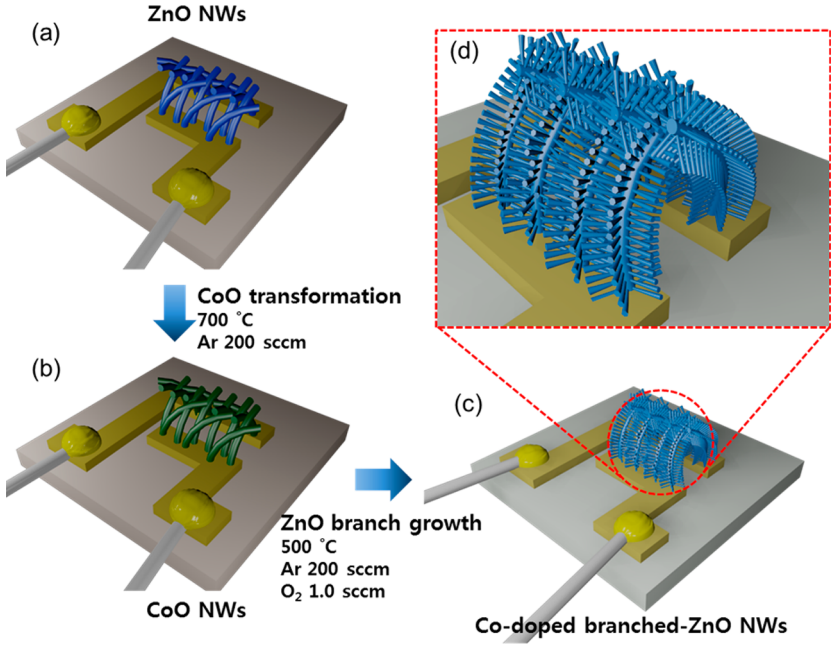

Figure 1. (a) Growth of ZnO NWs on alumina substrate with Au electrodes, (b) transformation of ZnO NWs into CoO NWs, (c, d) growth of Co-doped branched ZnO NWs from CoO NWs.

In the present work, we report a novel vapor-phase method to grow Co-doped branched ZnO NWs for the selective detection of *p*-xylene gas. The study is focused on the growth of branched ZnO NWs that results in a highly porous network structure, and the catalytic role of Co doping, which enabled the selective detection of *p*-xylene gas among various interfering gases, including C_2H_5OH, HCHO, benzene, and toluene.

2. EXPERIMENTAL SECTION

Sample Preparation. ZnO NWs were grown on alumina substrates (1.5 × 1.5 mm^2; thickness, 0.25 mm) with two gold electrodes (electrode length, 1 mm; separation, 0.2 mm) by thermal evaporation of a mixture of ZnO (99.9%. Sigma-Aldrich), graphite (<20 μm, Sigma-Aldrich), and Sn (99.8% Acros) powders (Figure 1a). The source powder (ZnO:graphite:Sn = 1:1:0.1 wt %) was loaded in an Al_2O_3 boat that was located at the center of a quartz tube (diameter: 2.5 cm), and the alumina substrates were placed 5 cm downstream from the source. The inside of the quartz tube was evacuated to ~9×10^{-2} Torr using a rotary pump, and the furnace temperature was increased to 900 °C. The ZnO NWs were grown for 20 min by the reaction between the source powder and a mixture of Ar−O_2 gas (Ar, 100 sccm; O_2, 0.2 sccm). The gold electrodes on the substrate acted as the catalyst for the vapor−liquid−solid (VLS) mechanism, which enabled the formation NW networks with highly porous structures and improved the connectivity between the NWs and the electrodes. The as-grown ZnO NWs were transformed into CoO NWs via the cation exchange reaction by thermal evaporation of $CoCl_2$ powder (99.9%, Sigma-Aldrich) at 700 °C (Figure 1b). The quartz tube was evacuated to ~9×10^{-2} Torr, and Ar (200 sccm) was flowed for 10 min. The CoO NWs were placed right next to the Zn powder (99.995% Sigma-Aldrich) in the Al_2O_3 boat that was placed at the center of the quartz tube in the horizontal furnace. After evacuating the tube using a rotary pump to ~9×10^{-2} Torr, the furnace was heated to 500 °C and was kept for 10 min under mixed Ar/O_2 gas (Ar, 200 sccm; O_2, 1.0 sccm). The corresponding reaction resulted in the growth of ZnO branches from the CoO NWs in which Co acted as growth catalyst for the VLS mechanism (Figure 1c,d).[10]

Characterization. The morphologies of pristine ZnO NWs, CoO NWs, and Co-doped branched ZnO NWs were analyzed using field emission scanning electron microscopy (FE-SEM, S-4800, Hitachi, Japan) and transmission electron microscopy (JEOL, JEM-2100F), the phase and crystallinity of the NWs by X-ray diffraction (XRD, Rigaku D/MAX-2500-V/PC), and the chemical state of the NWs by X-ray photoelectron spectroscopy (XPS, Thermo, MultiLab 2000).

Gas Sensing Characteristics. Sensors with directly grown NWs were heat-treated at 550 °C for 2 h before measuring their gas sensing characteristics. The sensors were placed in a quartz tube, and the temperature of the furnace was stabilized at 350−450 °C. A flow-through technique with a constant flow rate of 500 cm^3 min^{-1} was used. The gas concentration was controlled by changing the mixing ratio of the parent gases (5 ppm *p*-xylene, C_2H_5OH, toluene, trimethylamine (TMA), HCHO, NH_3, CO, benzene, and H_2) and dry synthetic air. The DC two-point probe resistance of the sensor was measured using an electrometer interfaced with a computer.

3. RESULTS AND DISCUSSION

Composition, and Structural, and Morphological Properties. Single crystalline ZnO NWs were grown on alumina substrates with two gold electrodes by the thermal evaporation method (Figure 2a,b). The diameters of the NWs ranged from 30 to 80 nm with several tens of micrometers in length (Figure 2c,d). The single crystalline ZnO NWs were grown along the $[01\bar{1}0]$ direction, as verified by the selected area electron diffraction (SAED) pattern (inset in Figure 2e) and the lattice-resolved image of $(01\bar{1}0)$ fringes separated by 2.81 Å (Figure 2f). The pristine ZnO NWs were transformed into CoO NWs by the thermal evaporation of $CoCl_2$ powders at 700 °C. The overall morphology and network configuration of the NWs remained similar (Figure 3a). The transformed CoO NWs were also highly crystalline (Figure 3b,c), and the lattice-resolved image showed (200) fringes separated by 2.13 Å (Figure 3d). The elemental mapping of Co, O, and Zn using energy-dispersive X-ray spectroscopy (EDS) (Figure 3e,f) confirmed that the pristine ZnO NWs were completely converted into CoO without any residual Zn. Highly pure Ar with an oxygen partial pressure of ~10^{-5} Torr was used as carrier gas. According to the phase diagram of the Co−O system, CoO is more stable than Co_3O_4 above 680 °C at this

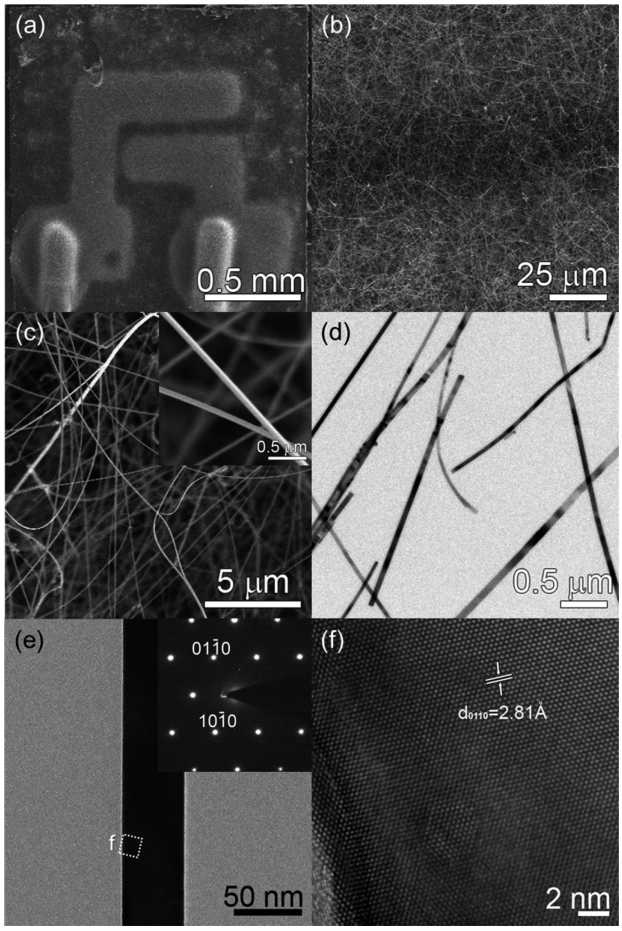

Figure 2. SEM (a–c) and TEM (d–f) images of pristine ZnO NWs.

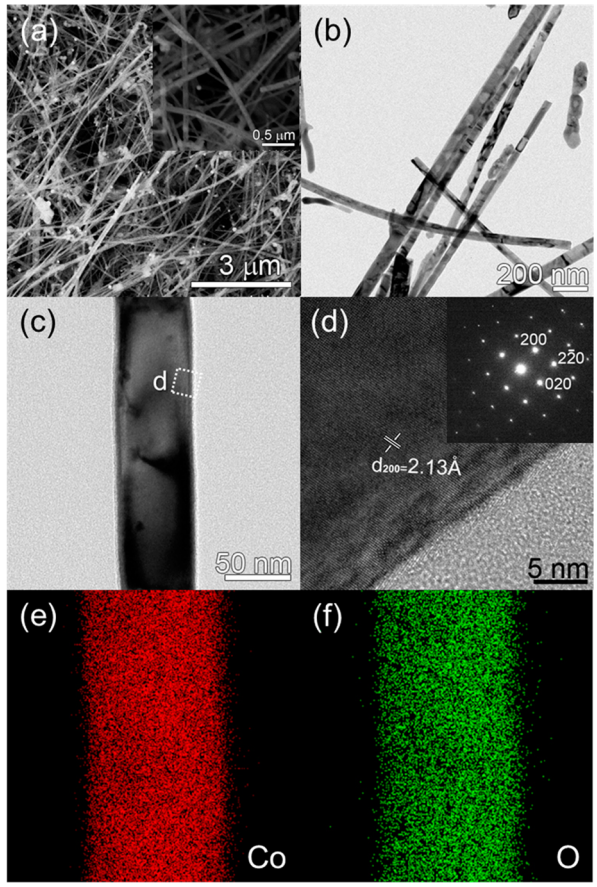

Figure 3. SEM (a) and TEM (b, c) images of CoO NWs, (d) lattice resolved image of the dotted area in (c) and corresponding SAED pattern (inset), and EDS elemental mapping of Co and O in CoO NW (e, f, respectively).

oxygen partial pressure.[11] This explains the formation of CoO NWs.

ZnO branches were directly grown on the CoO NWs by thermal evaporation of Zn powders at 500 °C (Figure 4a). In our previous work, CoO–ZnO core–shell NWs with ZnO branches were obtained at 450 °C.[12] With the growth temperature being increased by 50 °C, we found that hexagonal ZnO branches were uniformly grown on the CoO NWs while maintaining the porous network structure (Figure 4b,c). The ZnO branches typically started to grow with a narrow base attached to the stem, and became thicker as their length continued to extend up to about 1.3 μm. Although generally droplets of liquid alloy exist on the tip of NWs after VLS growth,[13] Hannon et al. reported that this is not always the case, stating that the consumption of catalyst eventually leads to the growth of smooth NWs.[14] Therefore, most of the Co seems to have been consumed for the growth of ZnO branches. Indeed, hexagonal facets are clearly visible at the tip of the branches (inset in Figure 4c), the thickness of which ranged from 100 to 500 nm (Figure 4d,e). The lattice-resolved image of a single branch shows highly crystalline (0002) fringes separated by 5.20 Å (Figure 4f), and the SAED pattern indicates that the branches were grown along the [0001] direction (inset of Figure 4f). It is a well-known fact that the surface energy of the polar (0002) surface is higher than that of the nonpolar (2$\bar{1}\bar{1}$0) and (01$\bar{1}$0) surfaces, which explains the preferential growth of ZnO nanostructures along the [0001] direction.[15,16] Unlike pristine ZnO NWs, which grew along the [01$\bar{1}$0] direction because of the Sn catalyst,[17,18] the ZnO branches grown by using Zn metal powder in the present study show the typical [0001] growth direction. The elemental mapping of Zn, O, and Co using EDS (Figure 4g–i) shows that residual Co exists uniformly within the ZnO lattice along the stem and the branches. This shows that the stems do not have a core–shell structure, but that CoO NWs were replaced almost completely by ZnO, which led to the formation of Co-doped branched ZnO. Such a multistep synthesis also improved the adhesion of the NWs to the Au electrodes on the sensor substrate, which greatly enhanced the stability of the gas sensor, resulting in high reproducibility.

Another interesting feature of the branched NWs is that the ZnO branches grew typically perpendicular to the backbone, which suggests that large ZnO [0001] surfaces were formed along the length of the stems during the conversion, similarly to the pristine NWs. The direct conversion of ZnO to CoO NWs is not associated with a unique relation between the crystal orientations of the two wurtzite and rock salt.[12] Nevertheless, CoO NWs typically exhibit fairly good crystallinity with [001] surfaces well developed along the NWs. This suggests that wurtzite [0001] faces transform to rock salt [001] during the conversion. The direct relation between the two surfaces is consistent with the phase transition mechanism between the two ZnO phases proposed by the first-principles calculations.[19,20] It is thus quite plausible that the wurtzite ZnO transforms to the rocksalt CoO via similar mechanisms. The single crystallinity of the NWs may further be compromised

dx.doi.org/10.1021/am506674u | ACS Appl. Mater. Interfaces 2014, 6, 22553–22560

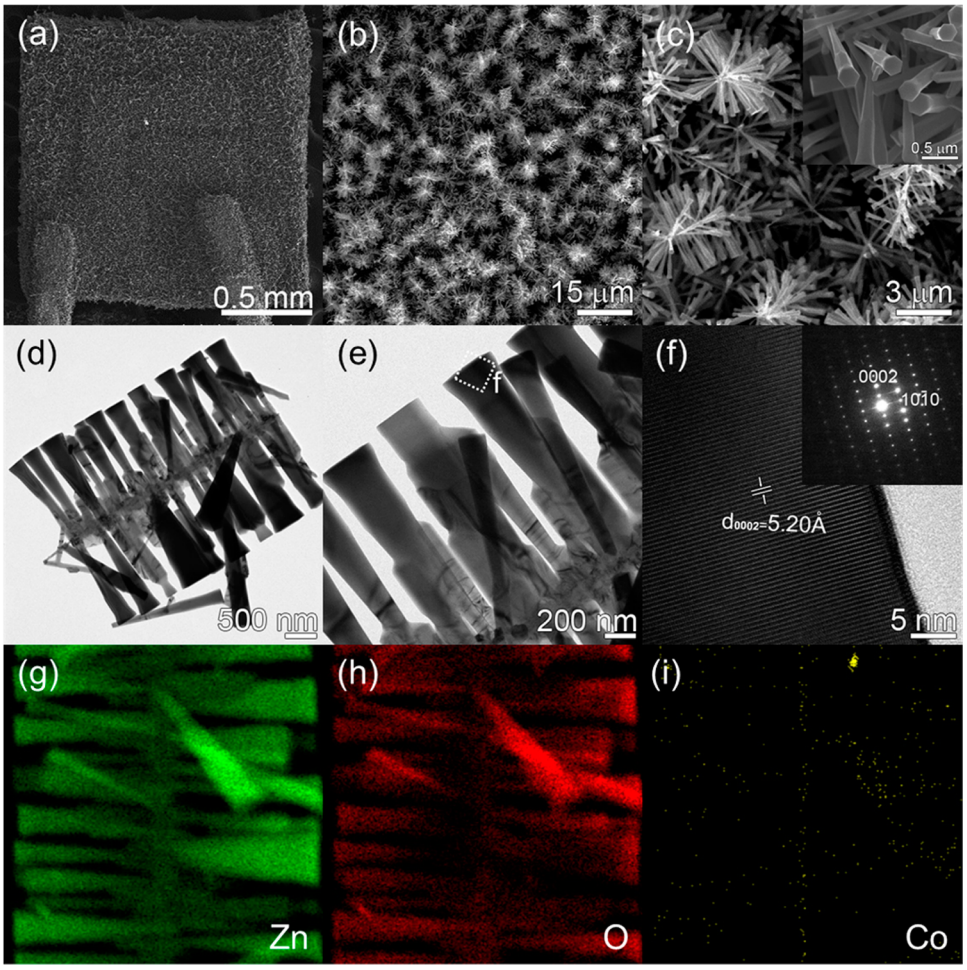

Figure 4. SEM (a–c) and TEM (d, e) images of Co-doped branched ZnO NWs, (f) lattice resolved image of the dotted area in (e) and corresponding SAED pattern (inset), and EDS elemental mapping of Zn, Co, and O in Co-doped branched ZnO NW (g–i).

during the reverse reactions converting CoO back to ZnO. It is very likely, however, that a significant percentage of the ZnO [0001] surfaces remains along the length of the NWs from where the ZnO branches grew out. Relatively small widths of the bases suggest that the stems are more or less polycrystalline in nature, including textures.

The pristine ZnO NWs were identified as wurtzite phase (JCPDS 36-1451), characterized by the primary ($10\bar{1}0$), (0002), and ($10\bar{1}1$) (Figure S1a, Supporting Information). Because of the decreased preferential growth of Co-doped branched ZnO NWs along the [0001] axis, the intensity of the (0002) peak decreased compared to that of pristine ZnO NWs grown along the [$01\bar{1}0$] axis. No Co-containing secondary phase was observed in the XRD analysis of the Co-doped branched ZnO NWs, probably resulting from the low detection limit of XRD (Figure S1b).

XPS analysis was carried out in order to verify the existence of Co and to determine its oxidation state in pure CoO and Co-doped branched ZnO NWs. Figure 5a shows the Zn 2*p* peaks of pristine ZnO, CoO, and Co-doped branched ZnO NWs. It is clear that no Zn $2p_{1/2}$ and/or Zn $2p_{3/2}$ peaks are visible after the transformation from ZnO to CoO NWs, but they reappear after the formation of ZnO branches. Both Zn $2p_{1/2}$ and Zn $2p_{3/2}$ peaks in the Co-doped branched ZnO NWs show shifting by 0.4 eV toward higher binding energy, which can be explained by the higher electronegativity (χ) of Co (χ = 1.88) compared

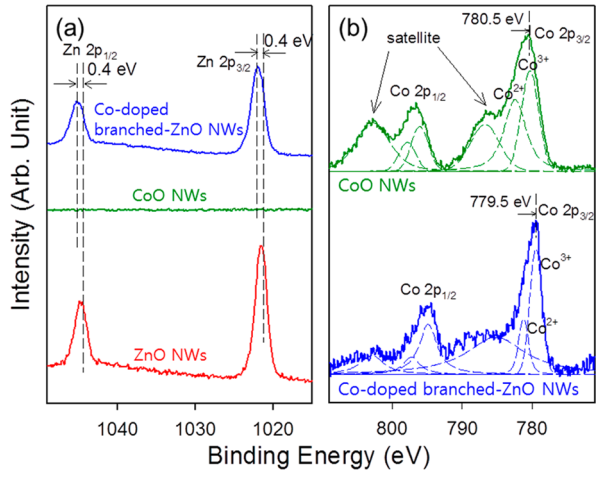

Figure 5. (a) Zn 2*p* XPS spectra of pristine ZnO, CoO, and Co-doped ZnO NWs, and (b) Co 2*p* XPS spectra of CoO and Co-doped ZnO NWs.

to that of Zn (χ = 1.65). Because of the higher electronegativity of Co, the electrons of Zn are attracted by Co, which decreases the electron screening effect for Zn,[21] thereby confirming doping of Co within the branched ZnO NWs.

The fine-scans of the Co 2*p* peaks of CoO and Co-doped branched ZnO NWs are shown in Figure 5b. The Co 2*p* peak

was deconvoluted into Co^{2+} and Co^{3+} peaks. Both Co^{2+} and Co^{3+} peaks were observed in all samples. Bulk CoO is stable at room temperature and atmospheric pressure, but Co_3O_4 is thermodynamically favorable under ambient conditions. Therefore, the spontaneous formation of Co_3O_4 at the surface of CoO NWs can be expected at room temperature and air atmosphere, which explains the existence of the Co^{3+} peak in CoO NWs.[22] From the fitting of the Co 2*p* peak using the Voigt amp method, the ratio of Co^{3+}/Co^{2+} of the CoO NWs was determined to be 0.78, which suggests that Co^{2+} is the major oxidation state. Likewise, the fitting of the Co 2*p* peak in Co-doped branched ZnO NWs using again the Voigt amp method resulted in the ratio of Co^{3+}/Co^{2+} of 1.24. This suggests that the majority of Co dopant within the branched ZnO NWs exists in the form of Co^{3+}. The Co concentration of the Co-doped branched ZnO NWs was 1.32 at.%, as determined by XPS.

Gas Sensing Characteristics. The gas sensing characteristics were measured in order to clarify the morphological and doping effect of Co-doped branched ZnO NWs. Both pure ZnO NWs and Co-doped branched ZnO NWs exhibited typical n-type gas sensing behaviors, characterized by the resistance decrease and increase upon exposure to reducing gas and air, respectively (Figure 6). All the samples were tested for their gas sensing characteristics toward 5 ppm *p*-xylene, toluene, C_2H_5OH, TMA, HCHO, NH_3, CO, benzene, and H_2 gases from 350 to 450 °C (Figure 7). The gas response ($S = R_a/R_g$: R_a, resistance in air; R_g, resistance in gas) of pure ZnO NWs toward 5 ppm of C_2H_5OH was the highest among all the gases throughout the entire sensing temperature range (S = 2.88–5.91) (Figure 7a). However, the gas responses toward C_2H_5OH were comparable to those of HCHO (S = 2.3–5.41), TMA (S = 2.64–3.96), and *p*-xylene (S = 1.79–5.03). The formation of branches and the doping of Co significantly enhanced the response to all the gases, but especially to 5 ppm *p*-xylene with the highest value of 20.25 at 375 °C (Figure 7b). This value is ~2.5 times higher than the responses to C_2H_5OH (S = 8.12) and toluene (S = 8.10). Although the Co-doped branched ZnO NWs showed the highest response and selectivity at 375 °C, the 90% recovery time after sensing *p*-xylene below 375 °C exceeded 1268 s, which was too long for in situ monitoring of gases. Accordingly, the optimum sensor temperature for the selective and sensitive detection of 5 ppm *p*-xylene gas with fast recovery can be regarded to be 400 °C, at which the response to 5 ppm *p*-xylene was 19.55. This value is 2.3 and 2.5 times higher than the responses to toluene and C_2H_5OH gases, respectively, and is significantly higher than the cross-references to other interference gases, such as TMA, HCHO, NH_3, CO, benzene, and H_2 (Figure 7b,c, and Figure S2, Supporting Information).

The sensing transients of Co-doped branched ZnO NWs to 0.25–5 ppm *p*-xylene were measured at 400 °C (Figure 8a). Not only is the response stable and reproducible, but also, by plotting the responses as a function of concentration, it is expected that the Co-doped branched ZnO NWs sensor can detect *p*-xylene gas at the sub-ppm level (Figure 8b). The resistances in air (R_a) of pristine ZnO NWs and Co-doped branched ZnO NWs from 350 to 450 °C are shown in Figure 8c. The substitution of Co within the ZnO lattice and the resulting electronic or ionic compensation proceed as follows:

$$Co_3O_4 \xrightarrow{3ZnO} Co_{Zn}^{\times} + 2Co_{Zn}^{\bullet} + 3O_O^{\times} + \frac{1}{2}O_2 + 2e^- \quad (1)$$

$$Co_3O_4 \xrightarrow{4ZnO} Co_{Zn}^{\times} + 2Co_{Zn}^{\bullet} + 4O_O^{\times} + \frac{1}{2}O_2 + V_{Zn}'' \quad (2)$$

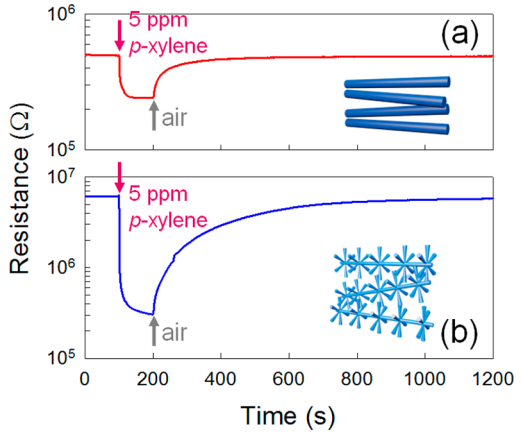

Figure 6. Sensing transients of (a) pristine ZnO and (b) Co-doped branched ZnO NWs to 5 ppm *p*-xylene at 400 °C.

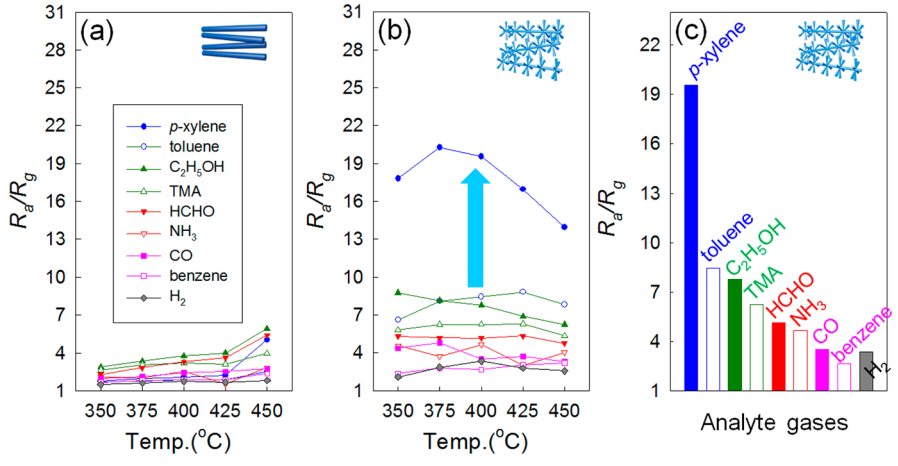

Figure 7. Gas response of (a) pristine ZnO and (b) Co-doped branched ZnO NWs to 5 ppm *p*-xylene, toluene, C_2H_5OH, TMA, HCHO, NH_3, CO, benzene, and H_2 at 350–450 °C; (c) gas selectivity of Co-doped branched ZnO NWs at 400 °C.

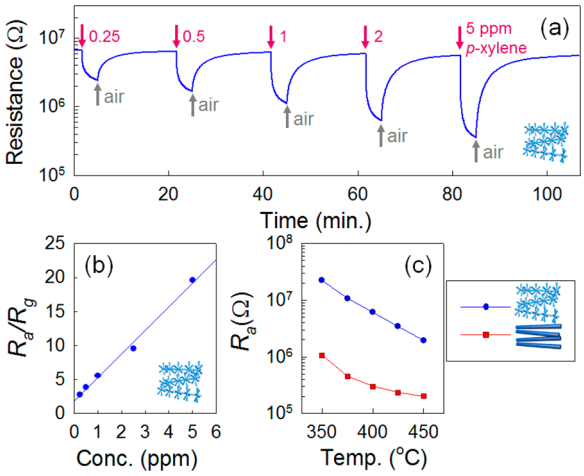

Figure 8. (a) Sensing transients of Co-doped branched ZnO NWs to 0.25−0.5 ppm *p*-xylene, (b) gas response to *p*-xylene as a function of concentration at 400 °C, and (c) resistance in air of pristine ZnO and Co-doped branched ZnO NWs from 350 to 450 °C.

Equation 1 shows the generation of electrons by Co^{3+} doping, in which the R_a value of ZnO should decrease rather than increase. The formation of Zn vacancies due to the incorporation of Co (eq 2) does not generate electrons or holes. Thus, the sensor resistance should remain similar in this case. However, by the formation of branches, the resistance has increased by 1.5 (450 °C) to 50 (350 °C) times (~12 times increase at 400 °C) compared to that of pristine ZnO NWs. According to reference studies and XPS analysis, the doping of Co in ZnO consists of both Co^{2+} and Co^{3+} with Co^{3+} as the major oxidation state.[23] The electronic sensitization, i.e., the enhancement of gas response due to the decrease in background charge carrier concentration by doping, can be considered as one possible reason to enhance the response.[28] However, according to eq 1, the charge carrier concentration increases rather than decreasing. Increasing the number of oxygen vacancies by either doping lower valence cations or annealing in a reducing atmosphere is known to enhance the gas response of ZnO NWs gas sensors.[24,25] In this perspective, the formation of Zn vacancy rather than oxygen by doping of Co^{3+} will not lead to the enhancement of gas response. The formation of nanoscale p−n junctions can also improve the gas sensor performance. In the present work, however, secondary phases such as p-type Co_3O_4 are absent in the XRD analysis and the EDS elemental mapping images, indicating that the Co content is likely doped within the branched ZnO NWs. Thus, the formation of nanoscale p−n junctions is less plausible. In oxygen adsorbed n-type NWs, Schottky potential barriers are formed at the contact points of NWs, similar to the grain-boundary contact model for nanoparticles. In order for conduction to occur, the current must pass through the depletion layers of two adjacent NWs at the contact points. Accordingly, the numerous inter-NW contacts per unit length in branched ZnO NWs results in the high R_a compared to pristine ZnO NWs.[26−28] In the serial connection between semiconducting NWs and resistive inter-NW contacts, the sensor response is dominated by chemiresistive variation in the electron depletion layers near the inter-NW contacts. This provides the morphological explanation for the enhanced gas responses in Co-doped branched ZnO.

The Co-doped branched ZnO NWs showed markedly higher response toward most gases compared to pristine ZnO NWs, especially to methyl benzenes. Many metal oxide semiconductors, such as ZnO, SnO_2, NiO, Co_3O_4, and In_2O_3, often show high response toward C_2H_5OH, probably because of their high reactivity.[29−33] This is also supported by the gas sensing characteristics of pristine ZnO NWs from the present work. Unlike C_2H_5OH, most n-type metal oxide semiconductor gas sensors show relatively low response toward methyl benzenes such as xylene and toluene, mainly due to their low reactivity. On the contrary, the Co-doped branched ZnO NWs gas sensor in the present study showed much higher response to methyl benzene compared to pristine ZnO NWs, especially to *p*-xylene. The amount of adsorbed oxygen on the surfaces of p-type oxide semiconductors, such as Co_3O_4, Cr_2O_3, NiO, and CuO, is known to be much larger compared to that of n-type metal oxides.[34] Therefore, most p-type oxide semiconductors are promising catalysts for the oxidation of less reactive VOCs.

Various metal oxide semiconductors, such as ZnO, SnO_2, CuO, WO_3, Cr_2O_3, Fe_2O_3, and TiO_2, have been explored with respect to the detection of methyl benzenes.[35−39] Most of these reports show either higher or similar response to ethanol, compared to methyl benzenes, which makes the selective detection of methyl benzenes difficult.[40−44] Recently, pure and Cr-doped Co_3O_4 and NiO have been reported to show selective detection of methyl benzenes with relatively low cross-responses to C_2H_5OH.[45,46] Co along with Mn and Br has been widely used for the catalytic liquid- and vapor-phase oxidation of *p*-xylene in the industrial production of fiber materials from low-cost petroleum.[6−9] Accordingly, the high response to *p*-xylene in Co-doped branched ZnO NWs can be attributed to the catalytic Co component that promotes the dissociation of the less reactive *p*-xylene to more reactive smaller gases.

Except for Co_3O_4, the selectivity toward xylene against interference from toluene ($S_{xylene}/S_{toluene}$) in the literature ranged from 1.02 to 1.44, which is still insufficient to discriminate two different gases.[47−49] In stark contrast, the $S_{xylene}/S_{toluene}$ value of the present sensor is as high as 2.3, indicating that the selective detection of xylene with negligible cross-responses to toluene and C_2H_5OH can be achieved. The distinction between the similar chemistry of *p*-xylene and toluene using oxide semiconductor gas sensors has been a challenging and important task. In this perspective, the present sensor using Co-doped branched ZnO NWs can be regarded as a novel new device that shows selective detection of *p*-xylene. However, the reason why the response to *p*-xylene is substantially higher than that to toluene is unclear and needs further study. The following can be considered as a plausible explanation. Even though xylene and toluene are both methyl benzenes, they differ by the number of methyl groups. Xylene, having one more methyl group than toluene, is known to be more reactive with a higher oxidation rate.[50,51] This is supported by Russell's report that the oxidation rate of *p*-xylene at 90 °C (0.0039 mol h^{-1}) is higher than that of toluene (0.0013 mol h^{-1})[52] and by the sensors in the literature showing slightly higher gas response to xylene than to toluene.[47−49] If the catalytic activity of the sensing material is too high, both xylene and toluene can be dissociated into smaller and more active species, which will lead to similar or comparable gas responses. On the other hand, if the catalytic activity of the sensing material is moderate, the gas sensing reaction toward relatively more reactive xylene will be preferentially promoted. In our previous report, the $S_{xylene}/S_{toluene}$ value of pure Co_3O_4

nanorods was as high as 1.89, whereas that of Cr-catalyst-doped Co_3O_4 nanorods was very low (1.01−1.07).[45] The addition of the Cr catalyst decreased the selectivity toward xylene, although it increased the response to toluene. Liu et al. also reported that a Co−ZnO composite nanofiber sensor showed selective detection of xylene with relatively low cross-response to toluene, although its response to *m*-xylene (S_{xylene} = 14.8−100 ppm) is lower than that of the present study (S_{xylene} = 19.55−5 ppm).[53] In this perspective, the moderate and tuned catalytic activity of the Co component within the Co-doped branched ZnO NWs is regarded as the reason for the highly selective detection of *p*-xylene.

4. CONCLUSION

The Co-doped branched ZnO NWs sensor was prepared using a three-step process, and it showed significantly improved response and selectivity to *p*-xylene gas with negligible cross-responses to other gases. On the other hand, pristine ZnO NWs showed the highest response to C_2H_5OH gas throughout the entire sensing temperature range. The enhancement of the gas response was explained by the increase in the number of chemiresistive contacts between ZnO branches, which is supported by the increase of the sensor resistance in air due to the formation of resistive Schottky barriers. The selective detection of *p*-xylene was attributed to the preferential dissociation of xylene into smaller and more reactive gases because of the moderate and tuned catalytic activity of the Co component. This novel method for the formation of Co-doped ZnO branches using CoO NWs as catalyst for VLS growth enabled the design of a highly sensitive, selective, and reproducible *p*-xylene gas sensor.

■ ASSOCIATED CONTENT

Ⓢ Supporting Information

X-ray diffraction patterns of pristine ZnO and Co-doped branched ZnO NWs, and gas sensing transients of Co-doped branched ZnO NWs. This material is available free of charge via the Internet at http://pubs.acs.org.

■ AUTHOR INFORMATION

Corresponding Author

*E-mail: jongheun@korea.ac.kr. Fax: +82-2-928-3584. Tel: +82-2-3290-3282 (J.-H.L.).

Notes

The authors declare no competing financial interest.

■ ACKNOWLEDGMENTS

This work was supported by the National Research Foundation of Korea (NRF) grant funded by the Korea Government (MEST) (No. 2013R1A2A1A01006545). J.-H.C. was independently supported by the ARCNEX (Grant No. 2011-0031933) from NRF of Korea funded by MEST.

■ REFERENCES

(1) Langenfeld, J. J.; Hawthorne, S. B.; Miller, D. J. Quantitative Analysis of Fuel-Related Hydrocarbons in Surface Water and Wastewater Samples by Solid-Phase Microextraction. *Anal. Chem.* **1996**, *68*, 144−155.

(2) Karlitschek, P.; Lewitzka, F.; Bünting, U.; Niederkrüger, M. Detection of Aromatic Pollutants in the Environment by Using UV-Laser-Induced Fluorescence. *Appl. Phys. B: Laser Opt.* **1998**, *67*, 497−504.

(3) Hongyan, X.; Xiulin, L.; Deliang, C.; Mei, L.; Minhua, J. A Novel Method for Improving the Performance of ZnO Gas Sensors. *Sens. Actuators, B* **2006**, *114*, 301−307.

(4) Wen, W.; Wu, J.-M.; Wang, Y.-D. Large-Size Porous ZnO Flakes with Superior Gas-Sensing Performance. *Appl. Phys. Lett.* **2012**, *100*, 262111.

(5) Hübner, M.; Simion, C. E.; Tomescu-Stănoiu, A.; Pokhrel, S.; Barsan, N.; Weimer, U. Influence of Humidity on CO Sensing with p-type CuO Thick Film Gas Sensors. *Sens. Actuators, B* **2011**, *153*, 347−353.

(6) Raghavendrachar, P.; Ramachandran, S. Liquid-Phase Catalytic Oxidation of *p*-Xylene. *Ind. Eng. Chem. Res.* **1992**, *31*, 453−462.

(7) Bhattacharyya, S. K.; Gulati, I. B. Catalytic Vapo-Phase Oxidation of Xylenes. *Ind. Eng. Chem.* **1958**, *50*, 1719−1726.

(8) Burri, D. R.; Jun, K.-W.; Yoo, J. S.; Lee, C. W.; Park, S.-E. Combined Promotional Effect of CO_2 and Ni on Co/Mn/Br Catalyst in the Liquid-Phase Oxidation of *p*-Xylene. *Catal. Lett.* **2002**, *81*, 169−173.

(9) Hronec, M.; Hrabě, Z. Liquid-Phase Oxidation of *p*-Xylene Catalyzed by Metal Oxides. *Ind. Eng. Chem. Prod. Res. Dev.* **1986**, *25*, 257−261.

(10) Lee, C. K.; Lee, T. J.; Lyu, S. C.; Zhang, Y.; Ruh, H.; Lee, H. J. Field Emission from Well-Aligned Zinc Oxide Nanowires Grown at Low Temperature. *Appl. Phys. Lett.* **2002**, *81*, 3648−3650.

(11) Chen, M.; Hallstedt, B.; Gauckler, L. J. Thermodynamic Assessment of the Co-O System. *J. Phase Equilib.* **2003**, *24*, 212−227.

(12) Na, C. W.; Park, S.-Y.; Kim, S.-J.; Woo, H.-S.; Kim, H.-J.; Chung, J.-H.; Lee, J.-H. Controlled Transformation of ZnO Nanobelts into CoO/Co_3O_4 Nanowires. *CrystEngComm* **2012**, *14*, 3737−3741.

(13) Wu, Y.; Yang, P. Direct Observation of Vapor-Liquid-Solid Nanowire Growth. *J. Am. Chem. Soc.* **2001**, *123*, 3165−3166.

(14) Hannon, J. B.; Kodombaka, S.; Ross, F. M.; Tromp, R. M. The Influence of the Surface Migration of Gold on the Growth of Silicon Nanowires. *Nature* **2006**, *440*, 69−71.

(15) Wang, Z. L. Zinc Oxide Nanostructures: Growth, Properties and Applications. *J. Phys.: Condens. Matter.* **2004**, *16*, R829−R858.

(16) Liu, P.-L.; Siao, Y.-J. Ab Initio Study on Preferred Growth of ZnO. *Scr. Mater.* **2011**, *64*, 483−485.

(17) Gao, P. X.; Wang, Z. L. Substrate Atomic-Induced Anisotropic Growth of ZnO Nanowires/Nanorods by the VLS Process. *J. Phys. Chem. B* **2004**, *108*, 7534−7537.

(18) Ding, Y.; Gao, P. X.; Wang, Z. L. Catalyst-Nanostructure Interfacial Lattice Mismatch in Determining the Shape of VLS Grown Nanorwires and Nanobelts: A Case of Sn/ZnO. *J. Am. Chem. Soc.* **2004**, *126*, 2066−2072.

(19) Saitta, A. M.; Decremps, F. Unifying Description of the Wurtzite-to-Rocksalt Phase Transition in Wide-Gap Semiconductors: The Effect of *d* Electrons on the Elastic Constants. *Phys. Rev. B* **2004**, *70*, 035214.

(20) Cai, J.; Chen, N. First-Principles Study of the Wurtzite-to-Rocksalt Phase Transition in Zinc Oxide. *J. Phys.: Condens. Matter* **2007**, *19*, 266207.

(21) Bae, S. Y.; Choi, H. C.; Na, C. W.; Park, J. Influence of In Incorporation on the Electronic Structure of ZnO Nanowires. *J. Phys.: Condens. Matter* **2007**, *19*, 266207.

(22) Petitto, S. C.; March, E. M.; Carson, G. A.; Langell, M. A. Cobalt Oxide Surface Chemistry: The Interaction of CoO(100), Co_3O_4(110) and Co_3O_4(111) with Oxygen and Water. *J. Mol. Catal.* **2008**, *281*, 49−58.

(23) Fu, J.; Ren, X.; Yan, S.; Gong, Y.; Tan, Y.; Liang, K.; Du, R.; Xing, X.; Mo, G.; Chen, Z.; Cai, Q.; Sun, D.; Wu, Z. Synthesis and Structural Characterization of ZnO Doped with Co. *J. Alloys Compd.* **2013**, *558*, 212−221.

(24) Ahn, M.-W.; Park, K.-S.; Heo, J.-H.; Park, J.-G.; Kim, D.-W.; Choi, K. J.; Lee, J.-H.; Hong, S.-H. Gas Sensing Properties of Defect-Controlled ZnO-Nanowire Gas Sensor. *Appl. Phys. Lett.* **2008**, *93*, 263103.

(25) Liao, L.; Lu, H. B.; Li, J. C.; Liu, C.; Fu, D. J.; Liu, Y. L. The Sensitivity of Gas Sensor Based on Single ZnO Nanowire Modulated by Helium Ion Radiation. *Appl. Phys. Lett.* **2007**, *91*, 173110.
(26) Xu, C. X.; Tamaki, J.; Miura, N.; Yamazoe, N. Grain Size Effects on Gas Sensitivity of Porous SnO_2-Based Elements. *Sens. Actuators, B* **1991**, *3*, 147−155.
(27) Hwang, I.-S.; Kim, Y.-S.; Kim, S.-J.; Ju, B.-K.; Lee, J.-H. A Facile Fabrication of Semiconductor Nanowires Gas Sensor Using PDMS Patterning and Solution Deposition. *Sens. Actuators, B* **2009**, *161*, 594−599.
(28) Sysoev, V. V.; Goschnik, J.; Schneider, T.; Strlcov, E.; Kolmakov, A. A Gradient Microarray Electronic Nose Based on Percolating SnO_2 Nanowires Sensing Elements. *Nano Lett.* **2007**, *7*, 3182−3188.
(29) Kim, K.-M.; Kim, H.-R.; Choi, K.-I.; Kim, H.-J.; Lee, J.-H. ZnO Hierarchical Nanostructures Grown at Room Temperature and their C_2H_5OH Sensor Applications. *Sens. Actuators, B* **2011**, *155*, 745−751.
(30) Hwang, I.-S.; Choi, J.-K.; Woo, H.-S.; Kim, S.-J.; Jung, S.-Y.; Seong, T.-Y.; Kim, I.-D.; Lee, J.-H. Facile Control of C_2H_5OH Sensing Charateristics by Decorating Descrete Ag Nanoclusters on SnO_2 Nanowire Networks. *ACS Appl. Mater. Interfaces* **2011**, *3*, 3140−3145.
(31) Yoon, J.-W.; Kim, H.-J.; Kim, I.-D.; Lee, J.-H. Electronic Sensitization of the Response to C_2H_5OH of p-Type NiO Nanofibers by Fe Doping. *Nanotechnology* **2013**, *24*, 444005.
(32) Choi, K.-I.; Kim, H.-R.; Kim, I.-D.; Lee, J.-H. C_2H_5OH Sensing Characteristics of Various Co_3O_4 Nanostructures Prepared by Solvothermal Reaction. *Sens. Actuators, B* **2010**, *146*, 183−189.
(33) Kim, S.-J.; Hwang, I.-S.; Na, C. W.; Kim, I.-D.; Kang, Y.-C.; Lee, J.-H. Ultrasensitive and Selective C_2H_5OH Sensors Using Rh-Loaded In_2O_3 Hollow Spheres. *J. Mater. Chem.* **2011**, *21*, 18560.
(34) Iwamoto, M.; Yoda, Y.; Yamazoe, N.; Seiyama, T. Study of Metal Oxide Catalysts by Temperature Programmed Desorption. 4. Oxygen Adsorption on Various Metal Oxides. *J. Phys. Chem.* **1978**, *82*, 2564−2570.
(35) Cao, Y.; Hu, P.; Pan, W.; Huang, Y.; Jia, D. Methanal and Xylene Sensors Based on ZnO Nanoparticles and Nanorods Prepared by Room-Temperature Solid-State Chemical Reaction. *Sens. Actuators, B* **2008**, *134*, 462−466.
(36) Hernandez, P. T.; Naik, A. J. T.; Newton, E. J.; Hailes, S. M. V.; Parkin, I. P. Assessing the Potential of Metal Oxide Semiconducting Gas Sensors for Illicit Drug Detection Markers. *J. Mater. Chem. A* **2014**, *2*, 8952−8960.
(37) Huang, J.; Xu, X.; Gu, C.; Wang, W.; Geng, B.; Sun, Y.; Liu, J. Effective VOCs Gas Sensor Based on Porous SnO_2 Microcubes Prepared via Spontaneous Phase Segregation. *Sens. Actuators, B* **2012**, *173*, 599−606.
(38) Huang, J.; Xu, X.; Gu, C.; Yang, M.; Yang, M.; Liu, J. Large-Scale Synthesis of Hydrated Tungsten Oxide 3D Architectures by a Simple Chemical Solution Route and Their Gas-Sensing Properties. *J. Mater. Chem.* **2011**, *21*, 13283−13289.
(39) Seo, M.-H.; Yuasa, M.; Kida, T.; Huh, J.-S.; Yamazoe, N.; Shimanoe, K. Microstructure Control of TiO_2 Nanotubular Films for Improved VOC Sensing. *Sens. Actuators, B* **2011**, *154*, 251−256.
(40) Bai, Z.; Xie, C.; Zhang, S.; Zhang, L.; Zhang, Q.; Xu, W.; Xu, J. Microstructure and Gas Sensing Properties of the ZnO Thick Film Treated by Hydrothermal Method. *Sens. Actuators, B* **2010**, *151*, 107−113.
(41) Gu, C.; Xu, X.; Huang, J.; Wang, W.; Sun, Y.; Liu, J. Porous Flower-like SnO_2 Nanostructures as Sensitive Gas Sensors for Volatile Organic Compounds Detection. *Sens. Actuators, B* **2012**, *174*, 31−38.
(42) Liu, Y.; Jiao, Y.; Zhang, Z.; Qu, F.; Umar, A.; Wu, Z. Hierarchical SnO_2 Nanostructures Made of Intermingled Ultrathin Nanosheets for Environmental Remediation, Smart Gas Sensor, and Supercapacitor Applications. *ACS Appl. Mater. Interfaces* **2014**, *3*, 2174−2184.
(43) Yang, C.; Su, X.; Xiao, F.; Jian, J.; Wang, J. Gas Sensing Properties of CuO Nanorods Synthesized by a Microwave-Assisted Hydrothermal Method. *Sens. Actuators, B* **2011**, *158*, 299−303.
(44) Song, H.-J.; Jia, X.-H.; Qi, H.; Tang, X.-F.; Min, C.-Y. Flexible Morphology-Controlled Synthesis of Monodisperse α-Fe_2O_3 Hierarchical Hollow Microspheres and Their Gas-Sensing Properties. *J. Mater. Chem.* **2012**, *22*, 3508−3516.
(45) Jeong, H.-M.; Kim, H.-J.; Rai, P.; Yoon, J.-W.; Lee, J.-H. Cr-Doped Co_3O_4 Nanorods as Chemiresistor for Ultraselective Monitoring of Methyl Benzene. *Sens. Actuators, B* **2014**, *201*, 482−489.
(46) Kim, H.-J.; Yoon, J.-W.; Choi, K.-I.; Jang, H. W.; Umar, A.; Lee, J.-H. Ultraselective and Sensitive Detection of Xylene and Toluene for Monitoring Indoor Air Pollution Using Cr-Doped NiO Hierarchical Nanostructures. *Nanoscale* **2013**, *5*, 7066−7073.
(47) Luo, S.; Fu, G.; Chen, H.; Liu, Z.; Hong, Q. Gas-Sensing Properties and Complex Impedance Analysis of Ce-Added WO_3 Nanoparticles to VOC Gases. *Solid State Ionics* **2007**, *51*, 913−919.
(48) Zhu, B. L.; Xie, C. S.; Wu, J.; Zeng, D. W.; Wang, A. H.; Zhao, X. Z. Influence of Sb, In and Bi Dopants on the Response of ZnO Thick Films to VOCs. *Mater. Chem. Phys.* **2006**, *96*, 459−465.
(49) Zhu, B. L.; Xie, C. S.; Wang, W. Y.; Huang, K. J.; Hu, J. H. Improvement in Gas Sensitivity of ZnO Thick Film to Volatile Organic Compounds (VOCs) by Adding TiO_2. *Mater. Lett.* **2004**, *58*, 624−629.
(50) Strini, A.; Cassese, S.; Schiavi, L. Measurement of Benzene, Toluene, Ethylbenzene and *o*-Xylene Gas Phase Photodegradation by Titanium Dioxide Dispersed in Cementitious Materials Using a Mixed Flow Reactor. *Appl. Catal., B* **2005**, *61*, 90−97.
(51) Chuang, K. T.; Cheng, S.; Tong, S. Removal and Destruction of Benzene, Toluene and Xylene from Wastewater by Air Stripping and Catalytic Oxidation. *Ind. Eng. Chem. Res.* **1992**, *31*, 2466−2472.
(52) Russell, G. A. The Rates of Oxidation of Aralkyl Hydrocarbons. Polar Effects in Free Radical Reactions. *J. Am. Chem. Soc.* **1956**, *78*, 1047−1054.
(53) Liu, L.; Zhong, Z.; Wang, Z.; Wang, L.; Li, S.; Liu, Z.; Han, Y.; Tian, Y.; Wu, P.; Meng, X. Synthesis, Characterization, and *m*-Xylene Sensing Properties of Co-ZnO Composite Nanofibers. *J. Am. Ceram. Soc.* **2011**, *94*, 3437−3441.